Journal of ELECTRONIC MATERIALS, Vol. 46, No. 4, 2017
DOI: 10.1007/s11664-016-5152-7

Tailoring Microwave-Absorption Properties of Co_xNi_y Alloy/RGO Nanocomposites with Tunable Atomic Ratios

XIAOQIN GUO,[1,2,3] ZHONGYI BAI,[2] BIAO ZHAO,[1] RUI ZHANG,[1,2] and JINGBO CHEN[1,4]

1.—School of Materials Science and Engineering, Zhengzhou University, Zhengzhou 450001, China. 2.—Zhengzhou University of Aeronautics, Zhengzhou 450046, China. 3.—e-mail: guoxq@zzia.edu.cn. 4.—e-mail: chenjb@zzu.edu.cn

Co_xNi_y nanoparticles anchored on reduced graphene oxide (rGO) composites with different Co(0)/Ni(0) ratios were successfully prepared by a simple hydrothermal method. The morphology, structure, and magnetic and microwave electromagnetic properties of Co_xNi_y/rGO composites were characterized by the x-ray diffraction, Fourier transform infrared spectrometry, scanning electron microscopy, Raman spectroscopy and a vector network analyzer. The Co_xNi_y/rGO composites exhibited enhanced microwave absorption properties, which are attributed to the effective complementarities between dielectric loss and magnetic loss. For the Co_3Ni_1/rGO composite, the minimum reflection loss (RL_{min}) is −44.89 dB at 12.22 GHz with absorber thickness of 2.5 mm, and the effective absorption bandwidth of the reflection loss (RL) < −10 dB (indicating 90% attenuation) could achieve 5.61 GHz. It is believed that the Co_3Ni_1/rGO composite may be a promising candidate as a microwave absorber with the features of low density, strong absorption, wide band and low thickness.

Key words: Reduced grapheme oxide, Co_xNi_y nanoparticles, microwave absorption, dielectric loss, magnetic loss

INTRODUCTION

With the rapid development of technology, for example, radar systems and wireless communication tools being extensively used, electromagnetic (EM) interference has become a serious pollution problem, which is harmful to the electronic devices, the ecological environment and human health.[1,2] Research to seek high-efficiency microwave-absorbing materials has attracted much attention and become an important topic.[3,4,5] Moreover, the current microwave-absorbing materials are required to possess strong absorption, wide absorption frequencies, low weight, and anti-oxidation properties.[6,7]

Graphene, a single layer of sp^2-hybridized carbon atoms ranked in a two-dimensional lattice,[8] has attracted much attention owing to its unique electrical, mechanical, and thermal properties. Graphene's unique structure and specific properties determine its wide range of potential applications.[9] Unfortunately, graphene alone cannot achieve better microwave-absorption properties because of the mismatch between its relatively high dielectric loss and low magnetic loss.[10] Based on the electromagnetic complementary theory, constructing the magnetic composition into graphene is an effective strategy to improve microwave-absorption performance.

In previous papers, there have been many reports about the microwave-absorption properties of magnetic metals or compounds with graphene.[11,12,13,14,15] Zhang and co-workers did some work on the synthesis of the heterojunction of Fe_3O_4 with graphene, revealing that hybrid materials can enhance microwave-absorption properties. Kim et al.[13] reported a facile strategy for the direct and uniform deposition of a graphene/Co_3O_4 thin film onto a stainless steel substrate through cathodic deposition and the film was employed as an anode material for lithium ion batteries. Pan et al.[14] assembled hexagonal and cubic

(Received June 13, 2016; accepted November 16, 2016; published online November 28, 2016)

Co nanocrystals grown on graphene. In a word, some inorganic nanoparticles could be attached to graphene and formed graphene-based composite materials. Zhang et al.[15] prepared a ZnO/graphene nanocomposite by an aqueous solution and calcination route and investigated its microwave-absorption properties. Meanwhile, graphene-based composites can possess an enhanced microwave-absorption performance.[16]

Recently, Co or Ni nanospheres anchored on the reduced grapheme oxide nanocomposites with magnetic, electric, photoelectric, spintronic and catalytic properties have been well studied. On the one hand, magnetic Co or Ni nanostructures with different phases and sizes have been of great interest for EM-wave absorption applications due to their excellent magnetic properties.[14] On the other hand, as an important transition metal alloy, CoNi alloy has drawn increasing attention due to its potential applications in catalysts, magnetic recording and magnetic resonance imaging, and microwave absorption.[17,18,19,20] But there are few reports on the investigations of Co_xNi_y/rGO composites. In this work, different proportions of Co(0)/Ni(0) nanoparticles anchored on rGO composites were prepared by a simple hydrothermal method. Moreover, the effects of different ratios of Co(0)/Ni(0) on the crystalline structure, morphology and electromagnetic wave-absorbing properties were studied.

EXPERIMENTAL

Preparation of Co_xNi_y/rGO Composites

Briefly, the graphite oxide (GO) was prepared from natural graphite by a modified Hummers' method,[21] which was used as the original material for the synthesis of Co_xNi_y/rGO hybrid nanomaterials. Then, the Co_xNi_y/rGO composites were synthesized by a hydrothermal method. In this process, first, 40 mg GO was dispersed in 30 mL ethyl alcohol. Then, 1 mmol mixture of $CoCl_2{\cdot}6H_2O$ and $NiCl_2{\cdot}6H_2O$ (for the Co_1Ni_4/rGO composite, the mole ratio of Co^{2+} and Ni^{2+} is 1:4; for the other Co_xNi_y/rGO composites, the (x, y) is (1, 3), (3, 1), and (4, 1), respectively.) were dispersed into the mixture and the system was stirred for 30 min. After that, 0.1 mol NaOH was added to the mixture to make sure the pH was 13 (the mixture was stirred for 20 min). Lastly, 4 mL hydrazine hydrate was added slowly with stirring. After the reaction, the mixed solution was placed into tahe drying oven and kept at 180°C for 12 h. The final Co_xNi_y/rGO products were collected by centrifuge, washed and dried.

Characterization

The structural characterization of Co_xNi_y/rGO composites were analyzed by XRD (XRD-3, using a Cu Kα source, λ = 0.154056 nm; Beijing Purkinje General Instrument). Fourier transform infrared (FT-IR) spectra were tested with a Nicolet iS10 FTIR spectrometer in the range of 4000–500 cm^{-1}. The morphology and microstructure was characterized by SEM (JSM-7001F). The detection of the molecular structure of the sample was analyzed by Raman spectroscopy (the excitation sources of the laser was 532 nm; Lab RAM HR Evolution; HORIBA Scientific). The complex permittivity and permeability were measured at room temperature by an Agilent N5244A VNA in the frequency range of 1–18 GHz. The measured samples were prepared by dispersing Co_xNi_y/rGO composites into paraffin with a weight ratio of 40% and then pressing thjem into a ring with an outer diameter of 7.00 mm and an inner diameter of 3.04 mm.

RESULTS AND DISCUSSION

XRD measurements were used to investigate the phase composition and the crystalline structure of the samples. The XRD patterns of the GO and Co_xNi_y/rGO composites are shown in Fig. 1, from which it can be seen than a diffraction peak of 9.8° is gained, which corresponds to the (001) plane of GO. It is well known that the crystal structure of graphite is destroyed by the oxidation of potassium permanganate and concentrated sulfuric acid. In this process, the covalent bonds between C and O were formed and the –CH, –OH, –COOH, etc. were inserted on the surface of the graphite sheet and thus a new crystal structure is shown. In the reduction process, the GO was reduced by caustic soda and hydrazine hydrate and the (001) plane of graphite oxidation disappeared. As shown in Fig. 1b–e, three new peaks at 2θ = 44.3°, 51.7° and 76.3° is consistent with the (111), (200), (220) planes, which can be classified as face-centered cubic (fcc) nickel (JCPDS no. 04-0850).[22] In Fig. 1b and c, the three peaks at 2θ = 44.3°, 51.7° and 76.3° match face-centered cubic crystalline cobalt (JCDPS 15-0806).[22] In Fig. 1d and e, the diffraction lines at 2θ values of 41.5°, 44.3°, 47.5° can be seen, which can be indexed to the (100), (002) and (101) planes of the hexagonal close-packed (hcp) cobalt structure (JCPDS no. 89-4308).[17] No obvious oxide peaks were found in Fig. 1b–e. With increasing the proportion of Co(0)/Ni(0), the crystal form of the alloy has changed, and the hexagonal cobalt appears when the value of Co(0)/Ni(0) is 3:1 and 4:1. According to these results, the hexagonal close-packed cobalt structure presents a lamellar petal, and the special structure may contribute to the microwave-absorption properties.

It is well known that FT-IR can be used to indicate the degree of removal of oxygen-containing groups. Figure 2 shows the infrared spectra of GO (a) and Co_xNi_y/rGO composites (b–e). Graphite was oxidized and changed to GO by potassium permanganate and concentrated sulfuric acid. The stretching vibration of hydroxy (–OH) is at ~3442 cm^{-1}, and the stretching vibration of C=O is at ~1735 cm^{-1}.[23,24,25,26,27,28] Then, some oxygen-containing groups could be found

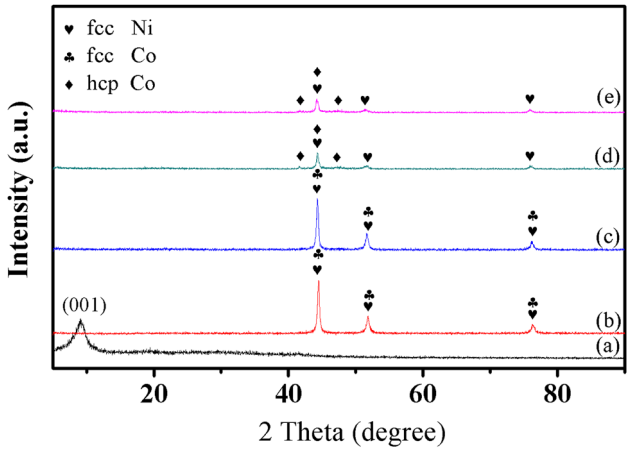

Fig. 1. XRD patterns of (a) GO, (b) Co_1Ni_4/rGO composite, (c) Co_1Ni_3/rGO composite, (d) Co_3Ni_1/rGO composite, (e) Co_4Ni_1/rGO composite.

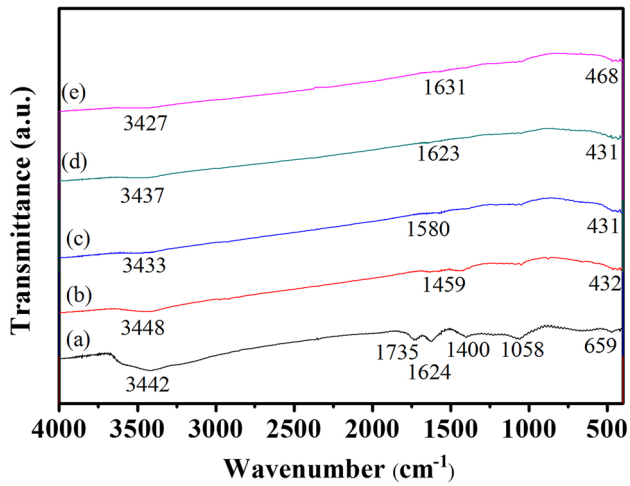

Fig. 2. FT-IR patterns of (a) GO, (b) Co_1Ni_4/rGO composite, (c) Co_1Ni_3/rGO composite, (d) Co_3Ni_1/rGO composite, (e) Co_4Ni_1/rGO composite.

in GO, which includes bands at ~1400 cm^{-1} (O–H stretching vibration of carboxyl), ~1058 cm^{-1} (C–O stretching vibration), and ~659 cm^{-1} (O–H stretching vibration of alcohol or phenol). The band at ~1624 cm^{-1} could be due to the unoxidized C–C graphite framework. But these oxygen-containing groups are almost completely removed by hydrazine hydrate in the reduction process. As shown in Fig. 2-b–e, the C–C of the graphite framework is indicated at the bands of ~1459 cm^{-1}, ~1580 cm^{-1}, ~1623 cm^{-1}, and ~1631 cm^{-1} respectively, while the different bands at ~431 cm^{-1}, ~432 cm^{-1}, and ~468 cm^{-1} are attributed to the lattice absorption of different proportions of the Co_xNi_y alloy, further affirming the existence of Co_xNi_y/rGO composites. In view of the above-mentioned data, we conclude that the GO is almost completely reduced.

The structures and morphologies of GO and Co_xNi_y/rGO composites were characterized by SEM, as shown in Fig. 3. In Fig. 3a, graphite has a fragmented distribution, and the layer thickness is thick. In Fig. 3b, it can be clearly seen that the pure GO has a flaky structure. At the edge of Fig. 3 GO, some burrs can be seen. Since the hydroxyl, carboxyl, epoxy and other oxygen-containing functional groups were introduced into Fig. 3 GO, the burrs formed and the spacing was increased in the sheet of GO.[29] In this phenomenon, GO cannot fully be reduced to the graphene structure during the reduction process, and some defects and oxygen groups remained. This fact may contribute to the microwave-absorption properties. As shown in Fig. 3c–f, Co_xNi_y nanocrystals were attached on the surface of the rGO sheets, and some nanocrystals were surrounded by the rGO.In Fig. 3c and d, the shape of the Co_xNi_y nanoclusters are spherical and schists. In Fig. 3e, Co_3Ni_1 alloy presents the petaloid-like structure. Meanwhile, the nanocrystals were uniformly attached on the surface of the rGO sheets. The morphology of the Co_4Ni_1/rGO composite is uneven, and the structure of the petaloid is incomplete. As the previous XRD described, the hexagonal cobalt phase has appeared in Fig. 3e and f. The hexagonal cobalt phase is always schistose and petaloid. Therefore, this morphology of the Co_xNi_y alloy is in accord with the data of XRD. According to reports, the shapes of schistose and petaloid and the homogeneity is favorable for the enhancement of microwave-absorption properties.

Raman spectroscopy is an effective method to judge ordered and disordered crystal structures of carbon-based materials.[24] Figure 4 shows the Raman spectra of the GO and Co_xNi_y/rGO composites. For the GO and composites, there are two characteristic peaks appearing at around 1350 cm^{-1} and 1597 cm^{-1}, which are attributed to the D and G bands.[30] The D band is a first-order zone boundary phonon mode associated with defects in the graphene or grapheme edge, while the G band is a radial C–C stretching mode of sp^2 bonded carbon.[24,31] The intensity ratio of D and G band (I_D/I_G) is a useful indicator to evaluate the ordered and disordered crystal structures of carbon.[30] The intensity ratios (I_D/I_G) are 0.93, 1.09, 1.14, 1.38, and 1.22 for the Co_xNi_y/rGO composites, respectively. These results indicated that the intensity ratio increased with increasing Co(0)/Ni(0), and the intensity ratio reaches a maximum when the Co(0)/Ni(0) is 3/1. Compared with GO, the intensity ratio for the Co_xNi_y/rGO composites shows a remarkable increase, which is caused by the decrease of the average size of the sp^2 domains and the increase of the disordered degree and the defects. It is suggested that a higher degree of defects in the composites result from the reduction of hydrazine hydrate and the introduction of the Co_xNi_y alloy, and that the defects play an important role in the enhancement of microwave-absorbing performance.[32,33] As shown in Fig. 4d, the intensity

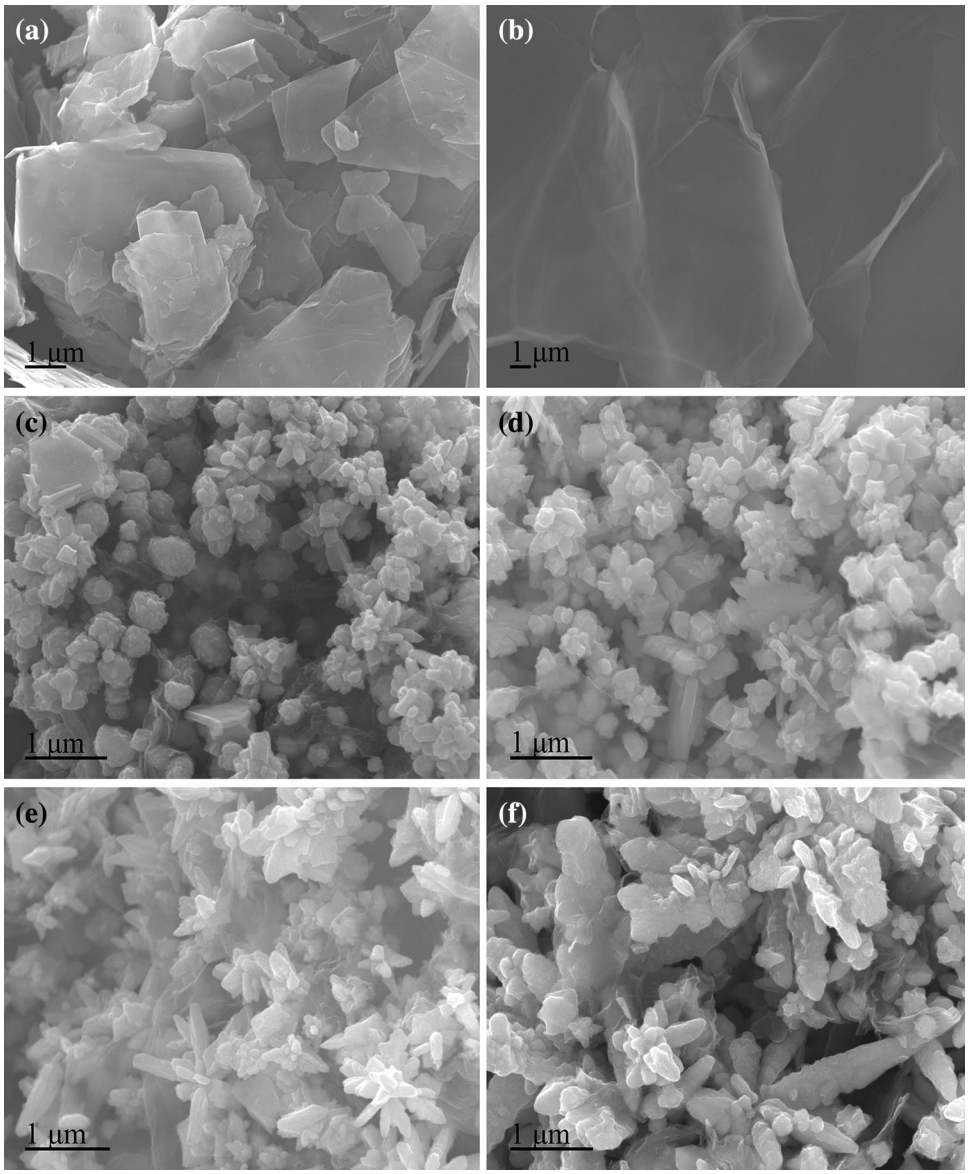

Fig. 3. SEM images of (a) graphite, (b) GO, (c) Co_1Ni_4/rGO composite, (d) Co_1Ni_3/rGO composite, (e) Co_3Ni_1/rGO composite, (f) Co_4Ni_1/rGO composite.

ratio of the Co_3Ni_1/rGO composite is 1.38, which indicates that the composite may possess better microwave-absorption properties.

The microwave-absorption properties of the Co_xNi_y/rGO composites can be estimated by the dielectric and magnetic properties. The relative complex permittivity ($\varepsilon_r = \varepsilon' - j\varepsilon''$) and the relative complex permeability ($\mu_r = \mu' - j\mu''$) of the Co_xNi_y/rGO composite microspheres have been measured in the frequency range of 1.0–18.0 GHz at room temperature. The real parts of the permittivity (ε') and permeability (μ') are associated with energy storage, while the imaginary parts of the permittivity (ε'') and permeability (μ'') are related to energy dissipation.[34]

In Fig. 5a, for the rGO and Co_xNi_y/rGO composites, the values of ε' are in the ranges of 17.55–6.10, 7.22–4.46, 8.94–4.59, 12.68–5.62 and 15.31–6.51 in the frequency of 1.0–18.0 GHz, respectively. Meanwhile, the values of ε'' are in the ranges of 22.68–4.24, 1.95–1.15, 4.45–1.54, 8.43–2.34 and 9.15–3.29 in the frequency of 1.0–18.0 GHz (Fig. 5b), respectively. It can be found that the samples with higher ratios (Co(0)/Ni(0)) show higher values of ε' and ε''. Obviously, both ε' and ε'' are decreased with the increase of the measured frequency, which may be caused by the defects and functional groups remaining in the Co_xNi_y/rGO composites. Figure 5c and d shows the μ' and μ'' values of the rGO and the Co_xNi_y/rGO composites. We can see that the value of

μ' is almost constant at 1.05 for the rGO, and the values of μ' are in the ranges of 1.23–1.00, 1.24–1.03, 1.24–1.04 and 1.21–1.00 for the Co_xNi_y/rGO composites in the frequency of 1.0–18.0 GHz, respectively. Meanwhile, the values of μ'' (Fig. 5d) are in the range of 0.01–0.07, 0.12–0, 0.12–0, 0.1–0.03 and 0.09–0.02 in the frequency of 1.0–18.0 GHz, respectively. From the above results, it can be found the μ' and μ'' of samples have the same trend in the whole frequency range. For the μ' of the samples, the Co_3Ni_1/rGO composite shows the highest values in the whole frequency range, which indicates that the composite has a better reservation capacity of magnetic energy. In addition, the μ'' exhibits multi-resonance peaks in the whole frequency range, which might be attributed to natural resonance and domain wall resonance.

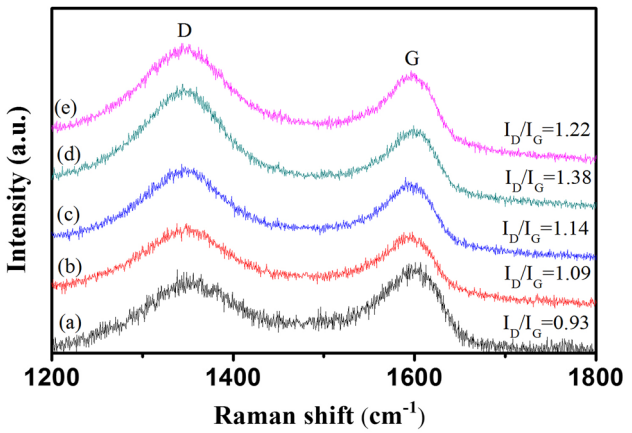

Fig. 4. Raman spectroscopy patterns of (a) GO, (b) Co_1Ni_4/rGO composite, (c) Co_1Ni_3/rGO composite, (d) Co_3Ni_1/rGO composite, (e) Co_4Ni_1/rGO composite.

The dielectric tangent loss ($\tan \delta_E = \varepsilon''/\varepsilon'$) and the magnetic tangent loss ($\tan \delta_M = \mu''/\mu'$) of the Co_xNi_y/rGO composites are shown in Fig. 6. For the Co_1Ni_4/rGO composite, the dielectric loss tangent shows an approximate constant around 0.3 over the whole frequency range, while the value of the magnetic loss tangent dramatically increases from 0.06 to 0.11 over the frequency range of 1.0–6.02 GHz. For the rGO and other Co_xNi_y/rGO composites, the values of the dielectric loss tangent are 1.29–0.67, 0.54–0.33, 0.78–0.43, 0.68–0.52, respectively, in the frequency of 1.0–18.0 GHz. For the magnetic loss tangent, the samples show strong fluctuation in the measured frequency. Amazingly, the values of

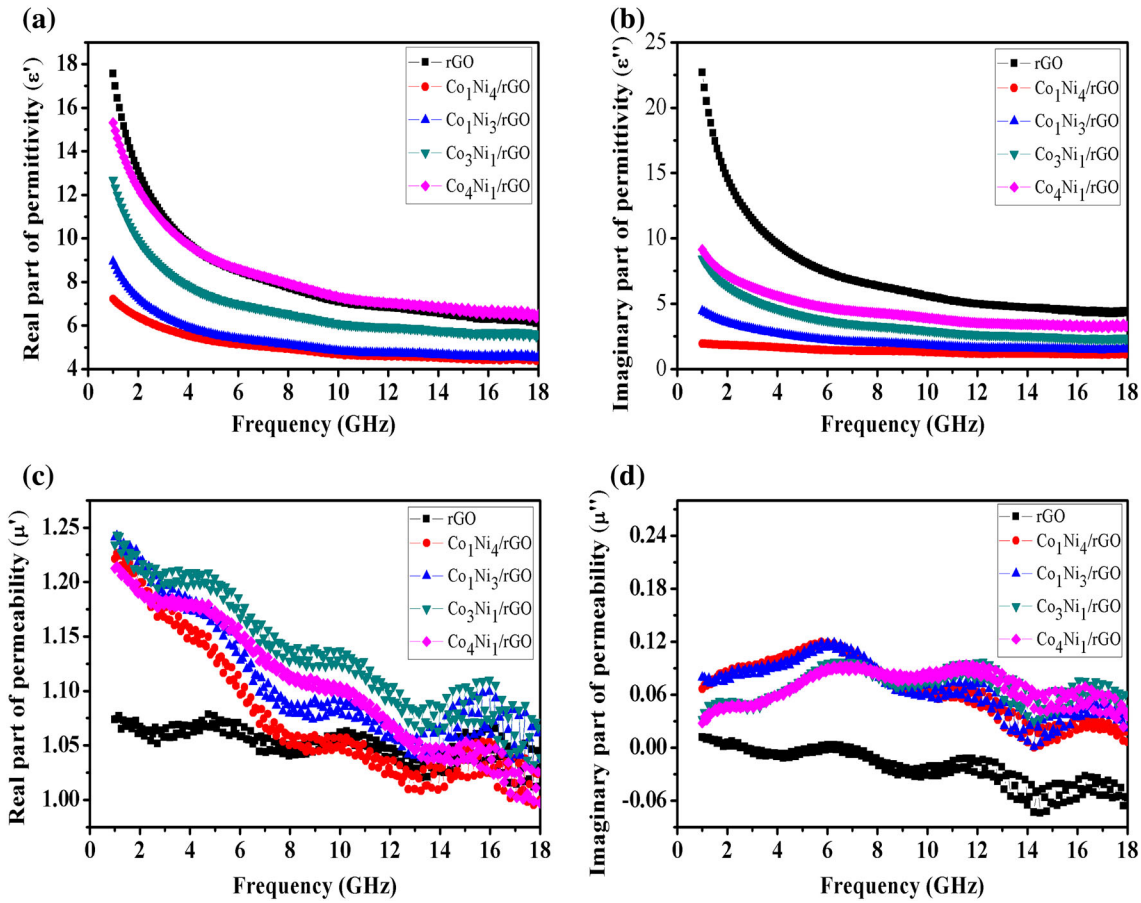

Fig. 5. Frequency dependence of (a) real part and (b) imaginary part of the relative complex permittivity, (c) real part and (d) imaginary part of the relative complex permeability of different Co_xNi_y/rGO composites.

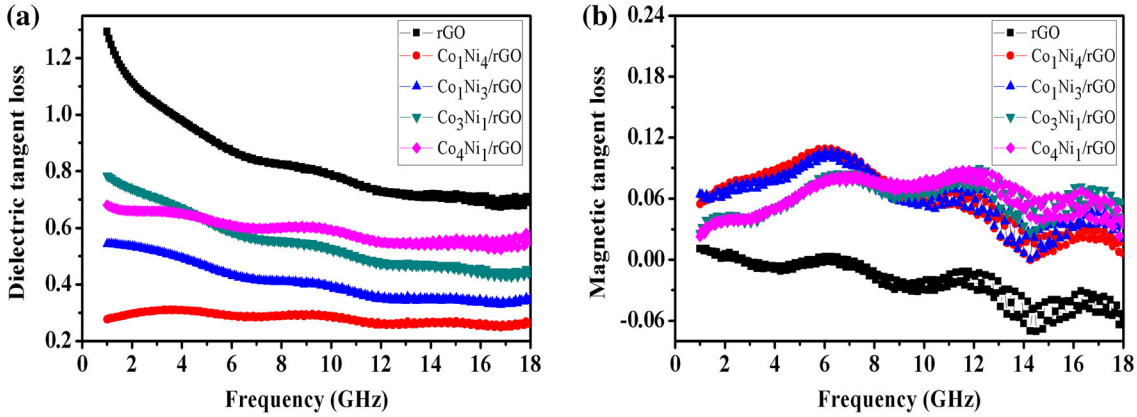

Fig. 6. The corresponding dielectric loss tangents (a) and magnetic loss tangents (b) of the different Co_xNi_y/rGO composites.

$\tan\delta_M$ for the rGO exhibit negative values, which correspond to the values of μ''. The tan δ_M exhibits multi-resonance peaks in the whole frequency range, which might be attributed to natural resonance and domain wall resonance. In the above results, the Co_1Ni_4/rGO composite shows the highest higher magnetic loss and relatively small magnetic loss in the measured frequency. It generally believed that high dielectric loss of microwave-absorption materials is not helpful in enhancement of the microwave-absorption property because it results in strong reflection and weak absorption.

The RL value is used to evaluate the EM wave absorption efficiency of absorbers (RL value of -10 dB is comparable to 90% of microwave absorption). The RL of the EM waves can be calculated using transmission theory[28,35,36]:

$$RL = 20\log_{10}|(Z_{in} - Z_0)/(Z_{in} + Z_0)| \quad (1)$$

$$Z_{in} = Z_0\sqrt{\frac{\mu_r}{\varepsilon_r}}\tanh\left(j\frac{2\pi fd\sqrt{\mu_r\varepsilon_r}}{c}\right) \quad (2)$$

where Z_0 is the impedance of free space, Z_{in} is the input characteristic impedance, μ_r is the complex permeability, ε_r is the complex permittivity, f is the frequency, c is the velocity of light, and d is the thickness of the Co_xNi_y/rGO composites. Figure 7 shows the relationship between the RL and frequency. It can be seen that the thickness of the absorber has a great influence on the properties of the microwave absorbtion, and that the RL_{min} of samples shifts toward lower frequency with the increase of thickness. Compared with the rGO and the Co_xNi_y/rGO composites, the Co_3Ni_1/rGO composite shows enhanced microwave-absorption properties. As shown in Fig. 7a, the RL_{min} reaches -17.39 dB at 14.26 GHz for rGO with a thickness of 2.0 mm, and a bandwidth of the RL < -10 dB (indicating 90% attenuation) could achieve 5.86 GHz from 12.14 GHz to 18 GHz. For the Co_1Ni_4/rGO composite (Fig. 7b), the RL_{min} reaches -10.56 dB at 12.22 GHz with a thickness of 3.0 mm, and a bandwidth of the RL < -10 dB could achieve 1.36 GHz from 11.46 GHz to 12.82 GHz. For the Co_1Ni_3/rGO composite (Fig. 7c), the RL_{min} reaches -15.24 dB at 11.80 GHz with a thickness of 3.0 mm, and a bandwidth of the RL < -10 dB could achieve 3.91 GHz, from 9.84 GHz to 13.75 GHz. For the Co_4Ni_1/rGO composite (Fig. 7e), the RL_{min} reaches -25.17 dB at 14.26 GHz with a thickness of 2.0 mm, and a bandwidth of the RL < -10 dB could achieve 6.29 GHz (from 11.71 to 18.00 GHz). Whereas for the Co_3Ni_1/rGO composite (Fig. 7d and f), the RL_{min} reaches -44.89 dB at 12.22 GHz with a thickness of 2.5 mm, and the effective absorption bandwidth of the RL < -10 dB could achieve 5.61 GHz, from 9.84 to 15.45 GHz. From the above results, the Co_3Ni_1/rGO composite shows the best microwave-absorption properties. Firstly, the hexagonal close-packed cobalt presents a lamellar-like structure, which contributes to the microwave-absorption properties. Secondly, the composites have a great amount of defects and oxygen groups, and these are regarded as polarization certers, which can cause a polarization relaxation process under the alternating electromagnetic field, resulting in a positive effect on the attenuation of microwave radiation.[6,7] Thirdly, an amount of particles loaded on the surface of rGO could introduce extra interfaces and cause more interfacial polarization. Lastly, large numbers of interfaces are formed between small-diameter and well-dispersed Co_3Ni_1 nanoparticles and the rGO. The existence of these interfaces generates interfacial polarization, which appears in heterogeneous media due to the accumulation of charges at the interfaces and the formation of dipoles on particles or clusters. So, these interfaces are responsible for the improvement of the microwave-absorption properties.

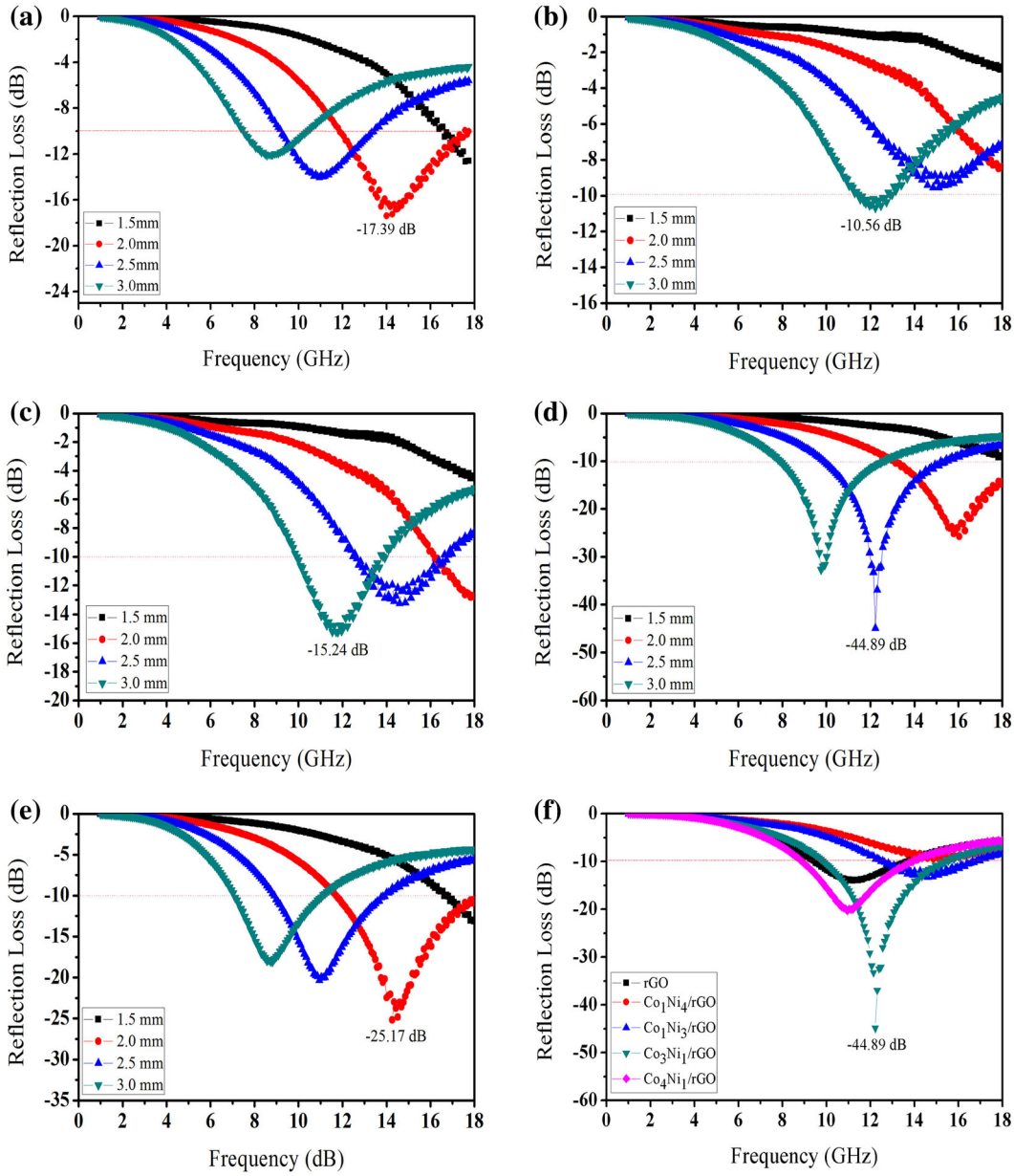

Fig. 7. Frequency dependence of (a) graphene, (b) Co_1Ni_4/rGO composite, (c) Co_1Ni_3/rGO composite, (d) Co_3Ni_1/rGO composite, (e) Co_4Ni_1/rGO composite and (f) the reflection loss for different Co_xNi_y/rGO composites with the thickness of 2.5 mm.

CONCLUSIONS

In summary, the different proportions Co_xNi_y nanoparticles anchored on the reduced graphene oxide composites were successfully prepared by a facile hydrothermal method. The results show that the Co_3Ni_1/rGO composite possesses outstanding microwave-absorption properties. The RL_{min} is −44.89 dB at 12.22 GHz for the corresponding thickness of 2.5 mm and the effective absorption bandwidth of RL < −10 dB (indicating 90% attenuation) could achieve 5.61 GHz. The results reveal that the Co_3Ni_1/rGO composite has practical applications in the microwave-absorption area.

REFERENCES

1. W. Zhang, S. Bie, H. Chen, Y. Lu, and J. Jiang, *J. Magn. Magn. Mater.* 1, 358 (2014).
2. C.J. Li and B. Wang, *J. Magn. Mater.* 1305, 324 (2012).
3. Y.P. Wang, D.P. Sun, G.Z. Liu, Y.J. Wang, and W. Jiang, *J. Electron. Mater.* 2292, 44 (2015).
4. C.L. Zhu, M.L. Zhang, Y.J. Qiao, G. Xiao, F. Zhang, and Y.J. Chen, *J. Phys. Chem. C* 16229, 114 (2010).
5. H.L. Yu, T.S. Wang, B. Wen, M.M. Lu, Z. Xu, C.L. Zhu, Y.J. Chen, X.Y. Xue, C.W. Sun, and M.S. Cao, *J. Mater. Chem.* 21679, 22 (2012).
6. H. Hekmatara, M. Seifi, and K. Forooraghi, *J. Magn. Magn. Mater.* 186, 346 (2013).
7. C. Zhou, Q. Fang, F. Yan, W. Wang, K. Wu, Y. Liu, Q. Lv, H. Zhang, Q. Zhang, J. Li, and Q. Ding, *J. Magn. Magn. Mater.* 1720, 324 (2012).

8. Y.W. Son, M.L. Cohen, and S.G. Louie, *Nature* 347, 444 (2006).
9. E.L. Ma, J.J. Li, N.Q. Zhao, E.Z. Liu, C.N. He, and C.S. Shi, *Mater. Lett.* 209, 91 (2013).
10. L. Kong, X. Yin, Y. Zhang, X. Yuan, Q. Li, F. Ye, L. Cheng, and L. Zhang, *J. Phys. Chem. C* 19701, 117 (2013).
11. Y.Q. Zhan, F.B. Meng, Y.J. Lei, R. Zhao, J.C. Zhong, and X.B. Liu, *Mater. Lett.* 1737, 65 (2011).
12. Y.Q. Zhan, R. Zhao, Y.J. Lei, F.B. Meng, J.C. Zhong, and X.B. Liu, *Appl. Surf. Sci.* 4524, 257 (2011).
13. G.P. Kim, I. Nam, N.D. Kim, J. Park, S. Park, and J. Yi, *Electrochem. Commun.* 93, 22 (2012).
14. G.H. Pan, J. Zhu, S.L. Ma, G.B. Sun, X.J. Yang, and A.C.S. Appl, *Mater. Interfaces* 1276, 5 (2013).
15. B.P. Zhang, C.X. Lu, and H. Li, *Mater. Lett.* 16, 116 (2014).
16. C. Hu, Z. Mou, G. Lu, N. Chen, Z. Dong, M. Hu, and L. Qu, *Phys. Chem. Chem. Phys.* 1308, 15 (2013).
17. B. Zhao, G. Shao, B.B. Fan, Y.J. Xie, and R. Zhang, *J. Magn. Magn. Mater.* 195, 372 (2014).
18. K.L. Wu, X.W. Wei, X.M. Zhou, D.H. Wu, X.W. Liu, Y. Ye, and Q. Wang, *J. Phys. Chem. C* 16268, 115 (2011).
19. R. Ferrando, J. Jellinek, and R.L. Johnston, *Chem. Rev.* 845, 108 (2008).
20. G. Kurlyandskaya, S. Bhagat, C. Luna, and M. Vazquez, *J. Appl. Phys.* 104308, 99 (2006).
21. W. Hummers Jr. and R.E. Offeman, *J. Am. Chem. Soc.* 1339, 80 (1958).
22. S. Rajasekhara, K. Ganesh, K. Hattar, J. Knapp, and P. Ferreira, *Scr. Mater.* 189, 67 (2012).
23. X.P. Shen, J.L. Wu, S. Bai, and H. Zhou, *J. Alloys Compd.* 136, 506 (2010).
24. H.L. Guo, X.F. Wang, Q.Y. Qian, F.B. Wang, and X.H. Xia, *ACS Nano* 2653, 3 (2009).
25. H.K. Jeong, Y.P. Lee, R.J.W.E. Lahaye, M.H. Park, K.H. An, I.J. Kim, C.W. Yang, C.Y. Park, R.S. Ruoff, and Y.H. Lee, *J. Am. Chem. Soc.* 1362, 130 (2008).
26. H.P. Cong, X.C. Ren, P. Wang, and S.H. Yu, *ACS Nano* 2693, 6 (2012).
27. C.Z. Zhu, S.J. Guo, Y.X. Fang, and S.J. Dong, *ACS Nano* 2429, 4 (2010).
28. X.Q. Guo, Z.Y. Bai, B. Zhao, R. Zhang, and J.B. Chen, *J. Mater. Sci.: Mater. Electron.* 8408, 27 (2016).
29. S. Pei and H.M. Cheng, *Carbon* 3210, 50 (2012).
30. L.L. Ren, S. Huang, W. Fan, and T.X. Liu, *Appl. Surf. Sci.* 1132, 258 (2011).
31. Y.Z. Xue, B. Wu, L. Jiang, Y.L. Guo, L.P. Huang, J.J. Chen, J.H. Tan, D.C. Geng, B.R. Luo, W.P. Hu, G. Yu, and Y.Q. Liu, *J. Am. Chem. Soc.* 11060, 134 (2012).
32. F.J. Zhang, J. Liu, K. Zhang, W. Zhao, W.K. Jang, and W.C. Oh, *Korean J. Chem. Eng.* 989, 29 (2012).
33. G.M. Rutter, J.N. Crain, N.P. Guisinger, T. Li, P.N. First, and J.A. Stroscio, *Science* 219, 317 (2007).
34. D.D. Zhang, D.L. Zhao, J.M. Zhang, and L.Z. Bai, *J. Alloys Compd.* 378, 589 (2014).
35. P.A. Miles and W.B. Westphal, *Rev. Mod. Phys.* 279, 29 (1975).
36. D. Chen, H. Quan, G.S. Wang, and L. Guo, *Chemplus Chem.* 843, 78 (2013).